Cyclodextrin nanosponge as a temoporfin nanocarrier: Balancing between accumulation and penetration in 3D tumor spheroids

Ilya Yakavets, Chloe Guereschi, Laureline Lamy, Irina Kravchenko, Henri-Pierre Lassalle, Vladimir Zorin, Lina Bezdetnaya

Version of Record: https://www.sciencedirect.com/science/article/pii/S0939641120301934
Manuscript_906ac154bd512221c91016db4c3c75e3

Cyclodextrin nanosponge as a Temoporfin nanocarrier: balancing between accumulation and penetration in 3D tumor spheroids

Ilya Yakavets [a,b,c,*], Chloe Guereschi [a,b], Laureline Lamy [a,b], Irina Kravchenko [c], Henri-Pierre Lassalle [a,b], Vladimir Zorin [c,d], Lina Bezdetnaya [a,b]

[a] Université de Lorraine, CNRS, CRAN, F-54500 Nancy, France;

[b] Institut de Cancérologie de Lorraine, 6 avenue de Bourgogne, 54519 Vandoeuvre-lès-Nancy, France

[c] Laboratory of Biophysics and Biotechnology, Belarusian State University, 4 Nezavisimosti Avenue, 220030 Minsk, Belarus;

[d] International Sakharov Environmental Institute, Belarusian State University, Dauhabrodskaja 23, 220030 Minsk, Belarus

*** Corresponding author**: i.yakavets@gmail.com; Tel.: +33-(0)3-08-59-83-53

Present/permanent address: 6 avenue de Bourgogne, 54519 Vandoeuvre-lès-Nancy, France

Abstract

As the intertissue delivery of hydrophobic temoporfin (mTHPC) remains inefficient, we propose the use of cyclodextrin-based nanosponges as a smart, advanced system for improved mTHPC delivery. Recently, we demonstrated that cyclodextrins (CDs) allow mTHPC to penetrate into tumor spheroids via a nanoshuttle mechanism. However, the CD complexes were very sensitive to the dilution, thus limiting their translation in vivo. Hypercrosslinked CD monomers in a three-dimensional network (namely, CD nanosponges), however, may form both inclusion and non-inclusion complexes with drug molecules, providing controlled release and prolonged exposure to the drug. In the present work, we demonstrate that epichlorohydrin-crosslinked CD nanosponges based on β-CD (βCDp) and carboxymethyl-β-CD (CMβCDp) monomers efficiently encapsulated mTHPC. We calculated the apparent binding constants between mTHPC and CD polymers ($K = (6.3–8.8) \times 10^6$ M^{-1} and $K = (1.2–1.7) \times 10^6$ M^{-1} for βCDp and CMβCDp, respectively) using fluorescence titration curve fitting. The encapsulation of mTHPC in a CD polymer matrix had slower photosensitizer (PS) release compared to monomer CD units, providing deep penetration of mTHPC in 3D tumor spheroids in a concentration-dependent manner. However, the improvement of mTHPC penetration in 3D human pharynx squamous cell carcinoma (FaDu) spheroids using CD polymers was strongly accompanied by the inhibition of PS cellular uptake, demonstrating the delicate balance between the accumulation and the penetration of PS in FaDu spheroids. In summary, mTHPC-loaded CD nanosponges are a strong candidate for further in vivo study in preclinical models, which could be considered as an advanced smart system for mTHPC delivery.

Keywords: temoporfin; cyclodextrin polymers; multicellular tumor spheroids; drug penetration; flow cytometry.

1. Introduction

Temoporfin (mTHPC; medicinal product name: Foscan®), is a potent clinically approved photosensitizer (PS) for the photodynamic therapy (PDT) of cancer [1]. Upon photoactivation, the photosensitizer generates reactive oxygen species, which are highly destructive, damaging such vital biomolecules as proteins, lipids, nucleic acids, and cell membranes [2]. Compared to traditional modalities, PDT offers a more targeted and less invasive treatment regimen [3]. Indeed, collateral PDT damage to healthy tissues can be minimized by selective PS accumulation in the target tissue, as well as by delivering the light in a spatially confined and focused manner [4]. On the other hand, optimal PDT treatment requires the accumulation of a sufficient PS concentration in tumor cells and, thus, deep penetration into the tumor tissue [4]. However, since most effective PSs, including mTHPC, tend to be insoluble hydrophobic molecules with a high tendency to aggregate, their encapsulation into nanocarriers is required for optimal PS distribution in tumor tissues [5–7].

To date, many nanoplatforms have been developed for mTHPC delivery [8]. Supramolecular complexes with cyclodextrins (CDs) stand out from other mTHPC-loaded nanomaterials due to the significant improvement in PS penetration in 3D tumor spheroids [9]. Cyclodextrins (CDs), owing to a toroidal structure with an inner hydrophobic cavity and outer hydrophilic surface, represent an excellent example of a supramolecular system [10]. CDs can improve the chemical and physical stability of drugs through the formation of drug/CD complexes [11], and can also modulate drug biodistribution when binding is strong enough [12]. It was demonstrated that β-CD derivatives exhibit an extremely high affinity to mTHPC, altering the in vitro mTHPC distribution in 2D monolayer cells, 3D tumor spheroids, and in vivo in xenografted mice [9,13]. However, the parental administration of inclusion complexes is accompanied by drug release upon dilution and rapid CD excretion from the circulating system [14].

In this context, we continue the application of promising CD technologies for mTHPC delivery by proposing CD-based nanosponges as potential nanocarriers. CD-based nanosponges, as a novel class of hyperbranched polymers, have gained considerable interest over the past decade [15]. The hypercrosslinking of CD monomers via linkers (e.g., epichlorohydrin) results in the formation of solid porous nanoparticles (nanosponges) within a three-dimensional network, forming both inclusion and non-inclusion complexes with drug molecules [16]. Nanosponge technology has been instrumental in achieving solubilization, sustained release, enhancement of bioavailability, and numerous other advantages [16]. To date, CD nanosponges have been intensively studied in pharmaceutics.

Dr. Trotta and collaborators intensively studied the use of CD nanosponges for the delivery of various anticancer drugs such as camptothecin [17,18], paclitaxel [19–21], tamoxifen [22], and doxorubicin [16,23] (extensively reviewed in [15]). In particular, they demonstrated the increase of camptothecin solubilization and modulation of its release upon encapsulation in CD nanosponges, resulting in the enhanced cytotoxicity of the CD nanoformulation toward cultured tumor monolayer cells in vitro [17,18]. Around the same time, Dr. Sortino and collaborators investigated the application of photoresponsive CD nanosponges in photodiagnosis (PD) and bimodal PDT upon encapsulation of PSs such as zinc phthalocyanine [24,25] and meso-tetrahydroxy-phenyl porphyrin (an mTHPC analog) [26]. Overall, the application of CD nanosponges offers an alternative to potentially toxic organic solvents, facilitating controlled drug release and could providing a good pharmacokinetic drug profile. Considering the extremely high affinity of CDs to mTHPC, we suggest that CD nanosponges may afford unique mechanisms for the modulation of mTHPC distribution in 3D tumor spheroids. To the best of our knowledge, this is the first report on the application of CD nanosponges as PS supramolecular carriers in 3D tumor spheroids.

With this aim, we investigated the binding of PS with epichlorohydrin-crosslinked polymers based on β-CD and carboxymethyl-β-CD monomers (Fig. 1), performing accurate

fluorescence titrations. The cellular accumulation of mTHPC-loaded CD polymers was assessed in human pharynx squamous cell carcinoma (FaDu) cells. Finally, we studied the relationship between the accumulation and penetration in 3D multicellular FaDu spheroids as a function of the CD polymer concentration.

2. Materials and methods

2.1. Materials

mTHPC and its liposomal formulation (Foslip®) were kindly provided by biolitec research GmbH (Jena, Germany). The stock solution of mTHPC (2 mM) was prepared in absolute ethanol and kept at 4 °C in the dark. For the in vitro cell experiments, stock solutions were diluted using phenol red-free Roswell Park Memorial Institute 1640 medium (RPMI-1640, Invitrogen™, Carlsbad, California, USA) supplemented with 2% heat-inactivated fetal bovine serum (FBS, Life Technologies, Carlsbad, California, USA) to obtain final concentrations of 1.5 µM for monolayer cells and 4.5 µM for tumor spheroids.

Randomly methylated β-cyclodextrin (Me-β-CD; product code CY-2004.1,29; substitution degree of 12; and average molecular weight 1135 Da), soluble carboxymethyl-β-cyclodextrin polymer (CMβCDp; catalog number: CY-2010), and soluble β-CD polymer (βCDp; catalog number: CY-2009) were purchased from CYCLOLAB R&D. Ltd., (Budapest, Hungary). As indicated by the manufacturer, both CMβCDp and βCDp are formulated by random crosslinking of the cyclodextrin monomers with epichlorohydrin and have the approximate molecular weight of 152 kDa (βCDp) and 153 kDa (CMβCDp) with an estimated cyclodextrin content of 50%–70%. The average degree of CMβCDp substitution was 3.0.

2.2. Cell lines

The FaDu (human pharynx squamous cell carcinoma) cell line was purchased from ATCC (Cat. No: ATCC1 HTB-43™). Cells were cultured in RPMI-1640 medium supplemented with 9% (v/v) heat-inactivated FBS, penicillin (10,000 IU), streptomycin (10,000 mg/mL), and 1% (v/v)

glutamine (Invitrogen™, Carlsbad, California, USA). The cells were kept as a monolayer culture in a humidified incubator (5% CO_2) at 37 °C and reseeded every week to ensure exponential growth.

2.3. Spheroid formation

MCTS were generated from FaDu cells using the liquid overlay technique (LOT), as previously described [27]. Briefly, 100 µL of FaDu cells (5×10^4 cells/mL) and 100 µL of full RPMI-1640 medium were added to each well of a 96-well plate previously coated with 1% agarose (w/v in water), and cultured at 37 °C, 5% CO_2 for 5 days before being taken into experiments. Between 8 to 16 spheroids were used for each experimental condition.

For dissociation, the spheroids were transferred into a 12-well plate, washed twice with PBS, and further incubated with 0.025% trypsin (GIBCO™, ThermoFisher, Waltham, MA, USA) and 0.01% ethylenediaminetetraacetic acid (GIBCO™, ThermoFisher, Waltham, MA, USA). For complete trypsinization, the plate with spheroids was placed on a rotatory shaker (60 rpm) for 30 min in subdued light. After dissociation, the trypsin action was inhibited by the addition of 3 mL of complete culture medium (RPMI-1640, 9% FBS), and the cell suspension was centrifuged to a pellet (1500 rpm, 5 min) and further resuspended in fresh medium.

After 5 days in culture, the FaDu spheroids were exposed to mTHPC nanoformulations and embedded into a resin matrix Shandon™ Cryomatrix™ (ThermoFisher, Waltham, MA, USA) for further fluorescence imaging and/or immunochemistry analysis of cryosections (10 µm thick sections). The spheroids were cut in the sagittal plane in order to confirm the sphericity. For further analysis, we used cryosections with a diameter of the spheroid section of about 450 µm, corresponding to the central part of spheroid.

2.4. Fluorescence staining

To obtain a 2D monolayer cell culture, FaDu cells (1.5×10^4 cells/mL) were seeded in 24-well plates for 72 h and then incubated with mTHPC (1 µg/mL) in the presence of various

concentrations of βCDp and CMβCDp. In the case of 3D cell culture, the spheroids were grown for 4 days, then 150 µL of complete medium was carefully removed from the plates and 200 µL of drug solution with CD polymers prepared in medium supplemented with 2% of serum was added to the spheroids to the final mTHPC concentration of 3 µg/mL. We used 8–16 spheroids per sample. The spheroids and monolayer cells were kept in a humidified incubator (5% CO2) at 37 °C in the dark.

2.5. Analytic techniques

2.5.1. Spectroscopy

The absorption measurements were recorded with a Lambda 35 spectrometer (Perkin Elmer, USA) and the fluorescence measurements were conducted with an LS55B spectrofluorometer (PerkinElmer, USA) and Solar CM 2303 (Solar, Belarus) equipped with polarizers, thermostated cuvette compartments, and magnetic stirring for the polarization experiments. The concentration of mTHPC in the solution was estimated by spectroscopy using a molar extinction coefficient of 29,600 $M^{-1}cm^{-1}$ at 650 nm in ethanol [28]. The fluorescence quantum yield (FQY) and fluorescence anisotropy (*r*) measurements were performed as described earlier [29]. The FQY of mTHPC in CD polymers was determined using the mTHPC solution in ethanol, regarded as the standard (the fluorescence quantum yield is equal to 0.092 [30]). For fluorescence anisotropy measurements, the mTHPC fluorescence was excited at 435 nm and measured at 652 nm. All measurements were carried out at room temperature.

The hydrodynamic diameter of CD polymers and the polydispersity index were determined using photon-correlated spectroscopy by Zetasizer Nano ZS (Malvern Instruments, UK). The samples were prepared in ultrapure water (Milli-Q® Advantage A10® System, Millipore, Eschborn, Germany) and filtered with 0.22 µm syringe filters (Millex®-GS, Merck Millipore Ltd., Cork, Ireland).

2.5.2. Calculation of binding constants

The global (macroscopic) apparent binding constants (*K*) were determined by fitting the titration curves using a custom MATLAB script (The Math Works, USA) [31] and applying a mathematical binding model (Eq. 1-2), which was previously described by Thordarson for 1:1 complexes [32]. For the optimization of the fit conditions, iterations were carried out until the difference in the value of chi-square for successive iterations did not exceed 5% of the previous value.

$$\Delta I = (K_{11}[CD])/(1 + K_{11}[CD]) \quad (1)$$

$$\Delta I = (I - I_0)/I_0 \quad (2)$$

where I_0 and I denote the fluorescence emission intensities of mTHPC in the absence and presence of CD polymers, respectively; K_{11} stands for the apparent binding constant; and [CD] is the concentration of the CD cavities.

2.5.3. Flow cytometry

Flow cytometry analysis was performed using FACSCalibur (BD, Franklin Lakes, NJ, USA), equipped with lasers emitting at 488 and 633 nm. The fluorescence of mTHPC was detected in the fluorescence channel FL4 with 661 ± 16 nm filter (λ = 633 nm). The mean fluorescence intensity (MFI) was used as a measure of the mean PS uptake in a 2D monolayer or 3D spheroid cell culture, while the shape (width) of distribution was quantified using the coefficient of variation (CV) and the ratio of the standard deviation (SD) to MFI. Data analysis was carried out using Flowing Software (Turku Centre for Biotechnology, Turku, Finland).

2.5.4. Cell Viability

The cell viability was assessed using MTT (3-(4,5-dimethylthiazol-2-yl)-2,5-diphenyl-2H-tetrazolium bromide; Sigma-Aldrich, St. Louis, MO, USA) colorimetric assay. The FaDu cells (1.5×10^4 cells/mL) were seeded in the 96-well plates, and 48 h later, the cells were washed twice with PBS and exposed to mTHPC (1.5 µg/mL) with and without CD polymers. After 24 h,

the medium was removed, MTT solution was added to each well, and the cells were kept in the humidified incubator for 3 h. The formazan crystals were solubilized by adding dimethyl sulfoxide and the absorbance was measured at 540 nm using a Multiskan Ascent spectrometer (Labsystems, TX, USA). From these values, the percentage of cell viability, compared to the control sample (no drug, no light) was calculated.

The viability of cells in 3D spheroids was assessed by histochemistry using HES (hematoxylin–eosin–safran) and an automated device (Dako CoverStainer, Dako, Santa Clara, CA, USA). For this purpose, the frozen sections were fixed for 1 min in 4% formaldehyde solution and rinsed with water before staining.

2.5.5. Fluorescence microscopy

The fluorescence imaging of spheroid cryosections was performed using an epifluorescence microscope (AX-70 Provis, Olympus, Tokyo, Japan) equipped with a 100 W mercury vapor lamp and a Peltier cooled CCD camera (DP72, Olympus, Tokyo, Japan). The filter was set at 400–440 nm bandpass excitation associated with a 570 nm dichroic mirror and a 590 nm longpass emission filter for the mTHPC fluorescence measurements.

The analysis of images was performed using ImageJ (NIH, USA) software. Custom macros for ImageJ were used to calculate the profile for dye penetration into the spheroids [27,33]. Briefly, the spheroid area was divided into 100 concentric rims with a linearly decreasing diameter. The mean intensity of the pixels in each rim was then calculated. The final profiles were plotted as the mean ± standard deviation from different cryosections (n = 6–9).

The depth corresponding to 50% PS distribution (d_{50}) was estimated for each profile using Origin software (OriginLab, Northampton, MA, USA). Briefly, the profile curve was integrated, normalized, and then the depth value that corresponded to 50% of the integral was taken as d_{50}.

2.5.6. Statistics

The data are reported as the mean ± standard deviation (SD) from at least three independent experiments. The test of normality of the data was carried out by performing the

Shapiro–Wilks W test. An unpaired, two-tailed Student's t-test with Welch correction was used for statistical analysis of the two groups (uptake dataset). One-way analysis of variance (ANOVA) followed by Tukey's multiple comparisons test was used for comparisons between three or more groups. The data analysis was carried out using Origin software (OriginLab, Northampton, MA, USA).

3. Results

3.1. Characterization

We studied the complex formation of mTHPC with two types of CD polymers based on β-CD and carboxymethyl-β-CD units crosslinked with epichlorohydrin. After 24 h of incubation of CD polymers in aqueous solution, mTHPC demonstrated monomeric behavior, namely narrow absorption peaks (Fig. 2A) and strong fluorescence (Fig. 2B). Compared to monomeric mTHPC in ethanol, the encapsulation of PS in CD polymers resulted in a slight decrease of the extinction coefficient of the Q_4 spectral band (ε_{650}), from 29,600 in ethanol [28] to 25,440 and 24,280 $cm^{-1}M^{-1}$ for mTHPC/CDp and mTHPC/CMβCDp, respectively (Table 1). At the same time, the FQY of mTHPC was higher in βCDp (0.107 ± 0.004, $p < 0.001$, $n = 4$) compared to CMβCDp (0.089 ± 0.005, $n = 4$) and ethanol (0.092) [30]. In addition, the anisotropy of the mTHPC fluorescence (r) was estimated as 0.147 ± 0.030 (βCDp) and 0.123 ± 0.010 (CMβCDp), revealing the encapsulation of mTHPC into the polymer matrix. Following from our previous study, the anisotropy of the mTHPC fluorescence in ethanolic solution was 0.02 [30].

The hydrodynamic size of the mTHPC-encapsulated polymers was measured by photon correlation spectroscopy (Table 2). The mean hydrodynamic diameter was 45.3 ± 8.1 nm for mTHPC/βCDp (PDI = 0.296 ± 0.106) and 59.3 ± 9.3 nm for mTHPC/CMβCDp (PDI = 0.454 ± 0.080). According to the manufacturer's data, the molecular weight (M_w) of the CD polymers is about 152 kDa, while β-CD and carboxymethyl-β-CD units have a weight of 1135 Da and 1391 Da, respectively. Considering that the cyclodextrin content was 50%–70%,

we can estimate that one CD polymer included 67–94 β-CD units or 56–78 carboxymethyl-β-CD units.

3.2. Binding with mTHPC

We further estimated the association constants of a complex formation between the mTHPC and CD polymers. The entrapment of mTHPC by CD polymers was studied by mTHPC titration with the different concentrations of βCDp and CMβCDp (until 345 µg/mL), corresponding to the concentration of 1.5–2.1 × 10^{-4} M of β-CD units and 1.3 ± 1.7 × 10^{-4} M of carboxymethyl-β-CD units (2.3 × 10^{-6} M polymer concentration). The range of the concentration of CD units (x-error) was calculated using the minimal cyclodextrin content of 50% and the maximal content as 70% in CD polymers. Figure 3A displays the titration curves obtained by measuring the mTHPC fluorescence intensity in aqueous solution after 24 h of incubation with various concentrations of CD polymers (presented in log scale).

Assuming a formal 1:1 complexation stoichiometry of mTHPC with CD units, the global apparent binding constants were determined by fitting the titration curves (R^2 = 0.98–0.99) (Fig. 3A). The CD polymers efficiently interacted with mTHPC with the apparent binding constants $K = (6.3–8.8) \times 10^6\ M^{-1}$ and $K = (1.2–1.7) \times 10^6\ M^{-1}$ for βCDp and CMβCDp, respectively (Table 3). Of note, the range of binding constants was calculated for both the minimal (50%) and maximal (70%) CD content in polymers. According to our calculations, we required almost a five-times higher concentration of CMβCDp compared to βCDp to bind a similar amount of PS molecules. In particular, mTHPC remained in the CD polymer matrix for a long time after dilution, slowing down PS release compared to unembedded mTHPC. Figure 3B represents the kinetics of mTHPC aggregation upon 100- and 1000-fold dilution of mTHPC-loaded CD polymers in PBS. As mTHPC is hydrophobic, its release from the CD polymers into the water was accompanied by the formation of non-fluorescent aggregates, resulting in a decrease in fluorescence intensity. After 1:100 dilution, the mTHPC fluorescence signal decreased 25% and 17% for βCDp and CMβCDp, respectively, after 3 h of incubation. The

1000-fold dilution resulted in a decrease of 40% and 33% for βCDp and CMβCDp, respectively. By comparison, the fluorescence intensity dropped down to 20% when inclusion complexes of mTHPC and monomeric Me-β-CD were diluted 1:100.

3.3. Cellular uptake of mTHPC in the 2D monolayer and 3D spheroid tumor models

FaDu monolayer cells were incubated with mTHPC in the presence of various concentrations of CD polymers, and the mTHPC cellular uptake was evaluated by flow cytometry. Results revealed that the incorporation of mTHPC into both βCDp and CMβCDp decreased the cellular uptake of the drug in FaDu cells in a CD concentration-dependent manner (Fig. 4). Indeed, in the presence of βCDp at 11.5 µg/mL, the intracellular content of mTHPC decreased to 50% compared to that of free mTHPC. Meanwhile, an equal drop in the mTHPC cellular uptake was achieved using only 34.5 µg/mL of CMβCDp. This result confirmed that the embedding of mTHPC inside CD polymers altered the PS distribution in cells, "masking" mTHPC molecules inside the CD nanosponge matrix. To confirm that the decrease in intracellular uptake was not related to cell viability, the MTT test was performed at the maximal (3450 µg/mL) CD polymer concentration used in the study. In fact, the cell viability was 106% ± 9% for mTHPC alone (1 µg/mL), while it was 85% ± 13% (n = 3, $p = 0.12$, ANOVA) and 75% ± 11% (n = 3, $p < 0.05$, ANOVA) in the presence of 3450 µg/mL βCDp and CMβCDp, respectively.

The accumulation of mTHPC between individual cells in the FaDu spheroids was also assessed by flow cytometry (Fig. S1). We demonstrated that mTHPC uptake was a function of the CD concentration, as observed for monolayer cells (Fig. 5). The total mTHPC cellular uptake was much lower in the presence of the βCDp polymer compared to an equal amount of CMβCDp. Indeed, a three-times higher concentration of CMβCDp compared to βCDp was required to achieve an identical decrease in mTHPC uptake. The complete inhibition of mTHPC uptake was demonstrated at 115 µg/mL of βCDp for 2D monolayer cells, while in the 3D spheroid model, a similar effect was observed at 1150 µg/mL of βCDp.

Additionally, to describe the evolution of mTHPC distribution histograms upon increasing the CD polymer concentration (Fig. S1), we used the coefficient of variation (CV) and the ratio of the standard deviation (SD) to the mean fluorescence intensity (MFI). In the absence of CD polymers, mTHPC demonstrated a wide multipeak distribution between the spheroid cells with a CV of 212 ± 37. The addition of βCDp enhanced the homogeneity of the mTHPC distribution resulting in a reduction of the CV value (63 ± 5 at 115 µg/mL). In the case of CMβCDp, the single-peak distribution of mTHPC (CV = 78 ± 7) was observed at a three-times higher concentration than that of βCDp (115 µg/mL). At a concentration of 115 µg/mL for any of the CD polymers, the CVs were 32 ± 6 and 48 ± 8 for βCDp and CMβCDp, respectively, corresponding to homogeneous single-peak distribution of PS between the spheroid cells, similar to the observations with monolayer culture (CV = 48 ± 6).

3.4. Penetration of mTHPC in 3D tumor spheroids

Generally, homogeneous distribution indicates deep penetration of PS across the spheroids. The penetration of mTHPC in 3D FaDu spheroids was assessed by fluorescence microscopy (Fig. 6A). The fluorescence imaging of cryosections of spheroids exposed to mTHPC demonstrated the peripheric distribution of PS, confirming the flow cytometry data. The addition of CD polymers resulted in the deeper penetration of mTHPC into the FaDu spheroids, accompanied by a gradual decrease in total PS fluorescence. According to the pseudocolored 3D surface plots, the complete penetration of mTHPC into the spheroids was observed at the concentrations of 34.5 and 115 µg/mL for βCDp and CMβCDp, respectively. The viability of FaDu spheroids was confirmed by HES staining of the cryosections (Fig. 6B).

For a better comparison of the mTHPC distribution in spheroids, the penetration profiles were calculated using a custom script in ImageJ (Fig. 7A). The profiles nicely illustrated the penetration of mTHPC into the spheroids as a function of the CD polymer concentration (Fig. 7B,C). For the quantitative analysis of the NP penetration, we calculated the depth along the radius in a spheroid, where the PS concentration was reduced by half, and denoted this as the

mid-penetration depth (d_{50}) (Fig. 7A). The estimated values represent the distance from the periphery of the spheroid, which is located at halfway point toward accumulated PS (Fig. 7D). The FaDu spheroids, as used in this study, were 427 ± 18 µm in diameter at 5 days post-seeding [27]. Hence, theoretically, in the case of the "ideal" uniform distribution of PS across the spheroid with a radius of 215 µm, the d_{50} should be close to 107 µm. According to our data, the d_{50} for mTHPC was 38.3 ± 14.2 µm. At the same time, the d_{50} values estimated for spheroids treated with mTHPC in the presence of βCDp were 65.3 ± 8.8, 81.3 ± 10.1, and 101.1 ± 6.1 µm for 11.5 , 34.5 , and 115 µg/mL, respectively.

For mTHPC–CMβCDp-treated spheroids, the d_{50} values were significantly higher than for mTHPC only ($p < 0.01$), and were equal to 61.4 ± 8.8, 73.8 ± 7.8, and 84.7 ± 6.5 µm for 34.5, 115, and 345 µg/mL, respectively. Considering the decrease in mTHPC uptake into spheroids upon the addition of CD polymers, we demonstrated a strong (negative) correlation between the penetration (d_{50} value) and the total PS accumulation (Pearson's correlation coefficient (PCC) of –0.893, $p < 0.01$) (Fig. 7E). In this way, we could significantly increase the penetration of mTHPC into the 3D spheroids at the cost of the total PS uptake. Hence, CD polymers offer an opportunity to modulate the balance between the uptake and penetration of PS in 3D tumor models.

4. Discussion

The results obtained in this study suggest that CD nanosponges can incorporate and deliver mTHPC to tumor tissues. Furthermore, CD nanosponges are likely to be less sensitive to dilution compared to CD monomers, enabling more prolonged exposure of the target tissues to mTHPC, thus have a promising future for in vivo applications of mTHPC/CD nanosponges. The CD nanosponges were well-tolerated and exhibited limited cytotoxicity at high concentrations (up to 3 mM), thus corroborating data from previously published studies [23,34,35]. We demonstrated that CD nanosponges could alter mTHPC accumulation in both FaDu monolayers and spheroid cells in a concentration-dependent manner. The loading of mTHPC into CD polymers led to a

significant reduction in cellular uptake, while the penetration depth in 3D tumor spheroids was concurrently increased upon addition of CD nanosponges.

According to our previous results, CDs mediate the penetration of mTHPC into HT29 spheroids [9]. We suggested that CDs act as nanoshuttles between serum lipoproteins and cellular membranes, thus accelerating the redistribution of lipophilic mTHPC through the aqueous media to the deep cell layers of spheroids. Recently, we reported complete penetration of mTHPC in HT29 and FaDu spheroids for "drug-in-cyclodextrin-in-liposome" formulation (mTHPC/CD nanoshuttles encapsulated into the liposomes) [36,37]. Indeed, CD/drug complexes are only a few nanometers in size, allowing them to diffuse into the spheroids. The penetration was deeper for CDs, which possess a higher affinity for mTHPC; thus, we hypothesized that the binding affinity played a key role in the nanoshuttle mechanism. In fact, strong binding (higher affinity constant) to the drug molecule slowed down the drug release from the complex, resulting in a longer lifetime of the complex and deeper penetration in the spheroids.

CD nanosponges consist of several dozens of CD monomers with an overall size of about 50 nm which, thus, likely limits their penetration. Despite their size, CD nanosponges efficiently delivered mTHPC to the center of the spheroids. This fact raises the question of the role of the binding affinity of CDs to mTHPC in CD-based PS delivery. The apparent binding constants for βCDp and CMβCDp with mTHPC were estimated as $K = (6.3–8.8) \times 10^6\ M^{-1}$ and $K = (1.2–1.7) \times 10^6\ M^{-1}$, similar to the association constant of monomeric Me-β-CD with mTHPC ($K = 7.1 \times 10^5\ M^{-1}$ [38]). The binding constants with β-CD monomers and CD polymers cannot be directly compared because (i) the constant for the monomers is based on the actual concentration of the host in solution while that of polymers is based on the average CD unit concentration; and (ii) crosslinked CD cavities are not equally accessible to mTHPC, while the binding constant neglects the actual organization of CD nanosponges. Thus, the binding constant for the β-CD unit within the nanoparticle may be underestimated. Nevertheless, we were still are able to compare the affinity to mTHPC for the CD polymers, namely βCDp, which possessed a

five-times higher affinity to mTHPC compared with CMβCDp (Fig. 3A). In summary, the CD polymers were observed to have a very high affinity for mTHPC ($K > 10^5\ M^{-1}$) and, thus, are expected to modulate its behavior in biological environments [12].

CD nanosponges possess a mesoporous structure, allowing them to form both inclusion and non-inclusion complexes with hydrophilic and hydrophobic compounds [35,39], thus increasing their binding capacity compared to CD monomers [40]. As mTHPC molecules could be localized in polymeric compartments [41,42], we considered the formation of both inclusion and non-inclusion complexes for mTHPC in CD polymers. The encapsulation of mTHPC was confirmed spectroscopically due to (i) narrow absorption peaks and strong fluorescence after 24 h in aqueous media in the presence of CD polymers (Fig. 2); and (ii) increased anisotropy of mTHPC fluorescence compared to the ethanolic solution (Table 1). Encapsulation of mTHPC in such a mesoporous structure prevented drug aggregation upon dilution (Fig. 3B). Thus, following a 1:1000 dilution, 60% of the mTHPC molecules remained monomeric in nanosponges versus 15% in the case of monomeric Me-β-CD (Fig. 3B). The monomerization effect of CDs was based on the recapturing of the released drug molecule by the closest available CD cavity. Thus, the local concentration of CD cavities was crucial to maintaining the monomeric state of PS. The CD polymers possessed a very high local concentration of CD cavities which was not affected by the dilution of the sample, compared to monomeric CDs.

Previous reports on the application of CD nanosponges as supramolecular carriers of PS have mainly focused on PS uptake in 2D monolayer cells at a single fixed concentration of CD polymers [24–26]. In the present work, we investigated, in detail, the mTHPC uptake in both 2D monolayers and 3D spheroid cell cultures as a function of the CD polymer concentration. We observed a gradual decrease in the intracellular mTHPC uptake upon increasing CD polymer concentrations in both the 2D and 3D in vitro models (Fig. 4). We supposed that the strong binding of PS molecules to the CD polymer matrix limited the accessibility of the drug to the cell membranes and could result in the inhibition of the cellular uptake in both the monolayers

and spheroid cells (Fig. 4). The addition of the CD polymer increased the probability of mTHPC encapsulation in CD nanosponges and slowed down the release; thus, we observed concentration-dependent inhibition of mTHPC uptake. Indeed, βCDp possessed a higher affinity compared to CMβCDp. In order to achieve the same level of mTHPC uptake, a three-times higher βCDp concentration was required. In the presence of CD polymers, the generally heterogeneous distribution of mTHPC between the individual spheroid's cells became almost homogeneous (Fig. 5).

Clearly, the homogeneous distribution indicates equal mTHPC access to every individual cell of the spheroid, illustrating complete PS penetration. Using flow cytometry analysis, we observed a decrease in the CV values upon increasing the concentration of CD polymers, representing the transition from a strongly heterogeneous distribution (CV > 150), corresponding to the initial mTHPC distribution in 3D spheroids, to an almost homogeneous single-peak distribution (CV = 40–70), corresponding to uniform accumulation in 2D cell cultures (Fig. 5B). These observations were confirmed by fluorescence microscopy of spheroid cryosections (Fig. 6) and advanced quantification analysis of the images (Fig. 7). Indeed, efficient intertissue delivery of hydrophobic mTHPC remains challenging [8]. mTHPC sequesters tightly in cells [43], significantly decreasing the probability of intracellular mTHPC distribution in spheroids and, as such, results in the heterogeneous accumulation of mTHPC only in the outermost peripherical cell layers (Fig. 6&7) [27,44,45]. At the same time, heterogeneous PS distribution could lead to insufficient PS accumulation in deep-seated tumors and can result in the relapse of in vivo tumor growth [46]. The mTHPC encapsulated in CD polymers diffused inside spheroids without interacting with peripherical cells, resulting in a smoother penetration profile (Fig. 7). In summary, balancing between the accumulation and penetration of mTHPC in the tissue can be achieved by varying the types and concentrations of CD polymer.

We propose that when the CD polymer concentration was increased: (i) more mTHPC molecules became bound to the CD nanosponges; (2) less mTHPC was delivered to the

peripherical cells; and (3) more mTHPC penetrated to the central cell layers of the spheroids. Such a mechanism explains the decrease in the total mTHPC accumulation along with the simultaneous increase in penetration depth, confirmed by a strongly negative PCC = (–0.893) (Fig. 7E). In this context, the strong PS binding inside CD nanosponges could be considered as an advantage. Compared to monomeric CDs with a similar affinity to mTHPC, the CD polymers exhibited slow drug release, thus providing deeper penetration. On the other hand, compared to the CD polymers based on CD units with a different affinity to mTHPC, the binding constant is a key parameter for determining the CD concentration required for the desired effect.

Our ongoing research is focused on the assessment of PDT efficacy of mTHPC-loaded CD nanosponges in 3D spheroids and in vivo preclinical models. The deeper penetration and homogenous distribution of the drug seem very promising for PDT studies; however, the uptake of a sufficient PS concentration in the tumor cells is also a crucial factor. Considering the strong correlation between the penetration and accumulation, we propose that mTHPC formulation based on CD nanosponges should be additionally optimized for PDT studies. Moreover, the saturation of CD nanosponges by preincubation with mTHPC would be preferable, in vivo, to improve the PS pharmacokinetic profile.

5. Conclusions

CD nanosponges enlarge the arsenal of CD-based delivery nanoplatforms for mTHPC delivery. They efficiently encapsulate mTHPC, providing drug solubilization upon dilution. According to the obtained data, CD nanosponges could be considered as modulators of mTHPC in both 2D monolayers and 3D spheroids in vitro tumor models. Despite their size (50 nm), CD polymers provide a unique opportunity to increase the penetration of mTHPC into the 3D spheroids at the cost of cellular uptake. We confirmed the critical role of the affinity constants in the CD-mediated delivery of mTHPC in 3D tumor spheroids. The results revealed the versatility of CD-based delivery nanoplatforms: we were able to modulate the biodistribution effect by varying the type and concentration of the CDs. This study suggests that CD nanosponges are a

strong candidate for in vivo studies in preclinical models, due to their limited toxicity, anticipated increase in mTHPC plasma lifetime, and most likely improved biodistribution profile compared to CD monomers [13]. We propose that CD nanosponges should be considered as an advanced smart system for mTHPC delivery.

6. Acknowledgments

This work was supported by the Institut de Cancérologie de Lorraine, French “Ligue Nationale contre le Cancer (CCIR-GE)”. The authors thank biolitec research GmbH (Jena, Germany) for providing with mTHPC. The authors thank Dr. Jordan Jasnieswki (Laboratoire d'Ingénierie des Biomolécules (LIBio), ENSAIA, Université de Lorraine) for the access to photon-correlated spectroscopy facilities.

7. References

[1] M.O. Senge, J.C. Brandt, Temoporfin (Foscan®, 5,10,15,20-tetra(m-hydroxyphenyl)chlorin)--a second-generation photosensitizer, Photochem. Photobiol. 87 (2011) 1240–1296. https://doi.org/10.1111/j.1751-1097.2011.00986.x.

[2] P. Agostinis, K. Berg, K.A. Cengel, T.H. Foster, A.W. Girotti, S.O. Gollnick, S.M. Hahn, M.R. Hamblin, A. Juzeniene, D. Kessel, M. Korbelik, J. Moan, P. Mroz, D. Nowis, J. Piette, B.C. Wilson, J. Golab, Photodynamic therapy of cancer: An update, CA. Cancer J. Clin. 61 (2011) 250–281. https://doi.org/10.3322/caac.20114.

[3] D.E.J.G.J. Dolmans, D. Fukumura, R.K. Jain, Photodynamic therapy for cancer, Nat. Rev. Cancer. 3 (2003) 380–387. https://doi.org/10.1038/nrc1071.

[4] A.P. Castano, T.N. Demidova, M.R. Hamblin, Mechanisms in photodynamic therapy: Part three-Photosensitizer pharmacokinetics, biodistribution, tumor localization and modes of tumor destruction, Photodiagnosis Photodyn. Ther. 2 (2005) 91–106. https://doi.org/10.1016/S1572-1000(05)00060-8.

[5] J. Kim, Y. Jo, K. Na, Photodynamic therapy with smart nanomedicine, Arch. Pharm. Res. 43 (2020) 22–31. https://doi.org/10.1007/s12272-020-01214-5.

[6] M. Abbas, Q. Zou, S. Li, X. Yan, Self-Assembled Peptide- and Protein-Based Nanomaterials for Antitumor Photodynamic and Photothermal Therapy, Adv. Mater. 29 (2017) 1605021. https://doi.org/10.1002/adma.201605021.

[7] A. Master, M. Livingston, A.S. Gupta, Photodynamic Nanomedicine in the Treatment of Solid Tumors: Perspectives and Challenges, J. Control. Release Off. J. Control. Release Soc. 168 (2013) 88–102. https://doi.org/10.1016/j.jconrel.2013.02.020.

[8] I. Yakavets, M. Millard, V. Zorin, H.-P. Lassalle, L. Bezdetnaya, Current state of the nanoscale delivery systems for temoporfin-based photodynamic therapy: Advanced delivery strategies, J. Controlled Release. 304 (2019) 268–287. https://doi.org/10.1016/j.jconrel.2019.05.035.

[9] I. Yakavets, I. Yankovsky, M. Millard, L. Lamy, H.-P. Lassalle, A. Wiehe, V. Zorin, L. Bezdetnaya, The alteration of temoporfin distribution in multicellular tumor spheroids by β-cyclodextrins, Int. J. Pharm. 529 (2017) 568–575. https://doi.org/10.1016/j.ijpharm.2017.07.037.

[10] T. Loftsson, P. Jarho, M. Másson, T. Järvinen, Cyclodextrins in drug delivery, Expert Opin. Drug Deliv. 2 (2005) 335–351. https://doi.org/10.1517/17425247.2.1.335.

[11] A. Popielec, T. Loftsson, Effects of cyclodextrins on the chemical stability of drugs, Int. J. Pharm. 531 (2017) 532–542. https://doi.org/10.1016/j.ijpharm.2017.06.009.

[12] V.J. Stella, Q. He, Cyclodextrins, Toxicol. Pathol. 36 (2008) 30–42. https://doi.org/10.1177/0192623307310945.

[13] I. Yankovsky, E. Bastien, I. Yakavets, I. Khludeyev, H.-P. Lassalle, S. Gräfe, L. Bezdetnaya, V. Zorin, Inclusion complexation with β-cyclodextrin derivatives alters photodynamic activity and biodistribution of meta-tetra(hydroxyphenyl)chlorin, Eur. J. Pharm. Sci. Off. J. Eur. Fed. Pharm. Sci. 91 (2016) 172–182. https://doi.org/10.1016/j.ejps.2016.06.012.

[14] V.J. Stella, V.M. Rao, E.A. Zannou, V. Zia, Mechanisms of drug release from cyclodextrin complexes, Adv. Drug Deliv. Rev. 36 (1999) 3–16. https://doi.org/10.1016/S0169-409X(98)00052-0.

[15] S. Swaminathan, R. Cavalli, F. Trotta, Cyclodextrin-based nanosponges: a versatile platform for cancer nanotherapeutics development, WIREs Nanomedicine Nanobiotechnology. 8 (2016) 579–601. https://doi.org/10.1002/wnan.1384.

[16] F. Trotta, M. Zanetti, R. Cavalli, Cyclodextrin-based nanosponges as drug carriers, Beilstein J. Org. Chem. 8 (2012) 2091–2099. https://doi.org/10.3762/bjoc.8.235.

[17] S. Swaminathan, L. Pastero, L. Serpe, F. Trotta, P. Vavia, D. Aquilano, M. Trotta, G. Zara, R. Cavalli, Cyclodextrin-based nanosponges encapsulating camptothecin: physicochemical characterization, stability and cytotoxicity, Eur J Pharm Biopharm. 74 (2010) 193–201. https://doi.org/10.1016/j.ejpb.2009.11.003.

[18] R. Minelli, R. Cavalli, L. Ellis, P. Pettazzoni, F. Trotta, E. Ciamporcero, G. Barrera, R. Fantozzi, C. Dianzani, R. Pili, Nanosponge-encapsulated camptothecin exerts anti-tumor activity in human prostate cancer cells, Eur J Pharm Sci. 47 (2012) 686–694. https://doi.org/10.1016/j.ejps.2012.08.003.

[19] B. Mognetti, A. Barberis, S. Marino, G. Berta, S. De Francia, F. Trotta, R. Cavalli, In vitro enhancement of anticancer activity of paclitaxel by a Cremophor free cyclodextrin-based nanosponge formulation, J. Incl. Phenom. Macrocycl. Chem. 74 (2012) 201–210. https://doi.org/10.1007/s10847-011-0101-9.

[20] K.A. Ansari, S.J. Torne, P.R. Vavia, F. Trotta, R. Cavalli, Paclitaxel loaded nanosponges: in-vitro characterization and cytotoxicity study on MCF-7 cell line culture, Curr. Drug Deliv. 8 (2011) 194–202. https://doi.org/10.2174/156720111794479934.

[21] S.J. Torne, K.A. Ansari, P.R. Vavia, F. Trotta, R. Cavalli, Enhanced oral paclitaxel bioavailability after administration of paclitaxel-loaded nanosponges, Drug Deliv. 17 (2010) 419–425. https://doi.org/10.3109/10717541003777233.

[22] S. Torne, S. Darandale, P. Vavia, F. Trotta, R. Cavalli, Cyclodextrin-based nanosponges: effective nanocarrier for tamoxifen delivery, Pharm. Dev. Technol. 18 (2013) 619–625. https://doi.org/10.3109/10837450.2011.649855.

[23] R. Cavalli, F. Trotta, W. Tumiatti, Cyclodextrin-based Nanosponges for Drug Delivery, J. Incl. Phenom. Macrocycl. Chem. 56 (2006) 209–213. https://doi.org/10.1007/s10847-006-9085-2.

[24] A. Fraix, N. Kandoth, I. Manet, V. Cardile, A.C.E. Graziano, R. Gref, S. Sortino, An engineered nanoplatform for bimodal anticancer phototherapy with dual-color fluorescence detection of sensitizers, Chem. Commun. 49 (2013) 4459–4461. https://doi.org/10.1039/C3CC40714D.

[25] A. Fraix, R. Gref, S. Sortino, A multi-photoresponsive supramolecular hydrogel with dual-color fluorescence and dual-modal photodynamic action, J. Mater. Chem. B. 2 (2014) 3443. https://doi.org/10.1039/c4tb00257a.

[26] M. Malanga, M. Seggio, V. Kirejev, A. Fraix, I.D. Bari, E. Fenyvesi, M.B. Ericson, S. Sortino, A phototherapeutic fluorescent β-cyclodextrin branched polymer delivering nitric oxide, Biomater. Sci. 7 (2019) 2272–2276. https://doi.org/10.1039/C9BM00395A.

[27] I. Yakavets, S. Jenard, A. Francois, Y. Maklygina, V. Loschenov, H.-P. Lassalle, G. Dolivet, L. Bezdetnaya, Stroma-Rich Co-Culture Multicellular Tumor Spheroids as a Tool for Photoactive Drugs Screening, J. Clin. Med. 8 (2019). https://doi.org/10.3390/jcm8101686.

[28] R. Bonnett, P. Charlesworth, B.D. Djelal, S. Foley, D.J. McGarvey, T.G. Truscott, Photophysical properties of 5,10,15,20-tetrakis(m-hydroxyphenyl)porphyrin (m-THPP), 5,10,15,20-tetrakis(m-hydroxyphenyl)chlorin (m-THPC) and 5,10,15,20-tetrakis(m-hydroxyphenyl)bacteriochlorin (m-THPBC): a comparative study, J. Chem. Soc. Perkin Trans. 2. (1999) 325–328. https://doi.org/10.1039/A805328F.

[29] I.V. Yakavets, I.V. Yankovsky, I.I. Khludeyev, H.P. Lassalle, L.N. Bezdetnaya, V.P. Zorin, Optical Methods for the Analysis of the Temoporfin Photosensitizer Distribution

Between Serum Proteins and Methyl-β-Cyclodextrin Nanocarriers in Blood Serum, J. Appl. Spectrosc. 84 (2018) 1030–1036. https://doi.org/10.1007/s10812-018-0582-z.

[30] I. Yakavets, I. Yankovsky, L. Bezdetnaya, V. Zorin, Soret band shape indicates mTHPC distribution between β-cyclodextrins and serum proteins, Dyes Pigments. 137 (2017) 299–306. https://doi.org/10.1016/j.dyepig.2016.11.007.

[31] I. Yakavets, yakavetsiv/binding-constant-matlab, 2020. https://github.com/yakavetsiv/binding-constant-matlab (accessed March 2, 2020).

[32] P. Thordarson, Determining association constants from titration experiments in supramolecular chemistry, Chem Soc Rev. 40 (2011) 1305–1323. https://doi.org/10.1039/C0CS00062K.

[33] I. Yakavets, yakavetsiv/Distribution, Git-Hub. (n.d.). https://github.com/yakavetsiv/Distribution (accessed March 2, 2020).

[34] J.-H. Park, K.-H. Choi, H.-S. Kwak, Single- and 14-day repeat-dose toxicity of cross-linked β-cyclodextrin in rats, Int. J. Toxicol. 30 (2011) 700–706. https://doi.org/10.1177/1091581811419678.

[35] S. Swaminathan, L. Pastero, L. Serpe, F. Trotta, P. Vavia, D. Aquilano, M. Trotta, G. Zara, R. Cavalli, Cyclodextrin-based nanosponges encapsulating camptothecin: Physicochemical characterization, stability and cytotoxicity, Eur. J. Pharm. Biopharm. 74 (2010) 193–201. https://doi.org/10.1016/j.ejpb.2009.11.003.

[36] I. Yakavets, H.-P. Lassalle, D. Scheglmann, A. Wiehe, V. Zorin, L. Bezdetnaya, I. Yakavets, H.-P. Lassalle, D. Scheglmann, A. Wiehe, V. Zorin, L. Bezdetnaya, Temoporfin-in-Cyclodextrin-in-Liposome—A New Approach for Anticancer Drug Delivery: The Optimization of Composition, Nanomaterials. 8 (2018) 847. https://doi.org/10.3390/nano8100847.

[37] I. Yakavets, M. Millard, L. Lamy, A. Francois, D. Scheglmann, A. Wiehe, H.-P. Lassalle, V. Zorin, L. Bezdetnaya, Matryoshka-Type Liposomes Offer the Improved Delivery of

Temoporfin to Tumor Spheroids, Cancers. 11 (2019) 1366. https://doi.org/10.3390/cancers11091366.

[38] I. Yakavets, H.-P. Lassalle, I. Yankovsky, F. Ingrosso, A. Monari, L. Bezdetnaya, V. Zorin, Evaluation of temoporfin affinity to β-cyclodextrins assuming self-aggregation, J. Photochem. Photobiol. Chem. 367 (2018) 13–21. https://doi.org/10.1016/j.jphotochem.2018.07.046.

[39] E. Gholibegloo, T. Mortezazadeh, F. Salehian, A. Ramazani, M. Amanlou, M. Khoobi, Improved curcumin loading, release, solubility and toxicity by tuning the molar ratio of cross-linker to β-cyclodextrin, Carbohydr. Polym. 213 (2019) 70–78. https://doi.org/10.1016/j.carbpol.2019.02.075.

[40] M.-C. Desroches, A. Kasselouri, O. Bourdon, P. Chaminade, J. Blais, P. Prognon, A direct sensitized fluorimetric determination of5,10,15,20-tetra(m-hydroxyphenyl)chlorin [m-THPC(Foscan)®] in human plasma using a cyclodextrin inclusion complex, Analyst. 126 (2001) 923–927. https://doi.org/10.1039/B100808K.

[41] V. Reshetov, D. Kachatkou, T. Shmigol, V. Zorin, M.-A. D'Hallewin, F. Guillemin, L. Bezdetnaya, Redistribution of meta-tetra(hydroxyphenyl)chlorin (m-THPC) from conventional and PEGylated liposomes to biological substrates, Photochem. Photobiol. Sci. 10 (2011) 911–919. https://doi.org/10.1039/C0PP00303D.

[42] V. Reshetov, V. Zorin, A. Siupa, M.-A. D'Hallewin, F. Guillemin, L. Bezdetnaya, Interaction of Liposomal Formulations of Meta-tetra(hydroxyphenyl)chlorin (Temoporfin) with Serum Proteins: Protein Binding and Liposome Destruction, Photochem. Photobiol. 88 (2012) 1256–1264. https://doi.org/10.1111/j.1751-1097.2012.01176.x.

[43] S. Mitra, T.H. Foster, Photophysical parameters, photosensitizer retention and tissue optical properties completely account for the higher photodynamic efficacy of meso-tetra-hydroxyphenyl-chlorin vs Photofrin, Photochem. Photobiol. 81 (2005) 849–859. https://doi.org/10.1562/2005-02-22-RA-447R.1.

[44] M. Millard, I. Yakavets, M. Piffoux, A. Brun, F. Gazeau, J.-M. Guigner, J. Jasniewski, H.-P. Lassalle, C. Wilhelm, L. Bezdetnaya, mTHPC-loaded extracellular vesicles outperform liposomal and free mTHPC formulations by an increased stability, drug delivery efficiency and cytotoxic effect in tridimensional model of tumors, Drug Deliv. 25 (2018) 1790–1801. https://doi.org/10.1080/10717544.2018.1513609.

[45] E. Gaio, D. Scheglmann, E. Reddi, F. Moret, Uptake and photo-toxicity of Foscan®, Foslip® and Fospeg® in multicellular tumor spheroids, J. Photochem. Photobiol. B. 161 (2016) 244–252. https://doi.org/10.1016/j.jphotobiol.2016.05.011.

[46] K. Haedicke, S. Gräfe, F. Lehmann, I. Hilger, Multiplexed in vivo fluorescence optical imaging of the therapeutic efficacy of photodynamic therapy, Biomaterials. 34 (2013) 10075–10083. https://doi.org/10.1016/j.biomaterials.2013.08.087.

Figure captions

Fig. 1. Schematic representation: i) CD crosslinking with epichlorohydrin; ii) loading of CD nanosponges with mTHPC

Fig. 2. (**A**) Absorbance and (**B**) fluorescence intensity (FI) of mTHPC (1 µg/mL) in ethanol (black), in complex with βCDp (blue) and in complex with CMβCDp (red). The fluorescence of mTHPC was excited at 420 nm. The concentration of CD polymers was 115 µg/mL.

Fig. 3. Binding of mTHPC (1 µg/mL) with CD polymers. (**A**) Titration curves of mTHPC by βCDp (●) and CMβCDp (♦) in PBS. Filled areas represent fitting (R^2 = 0.98-0.99) for mTHPC/βCDp (blue) and mTHPC/CMβCDp (red). Values are the mean ± SD of 3 separate evaluations. (**B**) Kinetics of mTHPC aggregation upon dilution of inclusion complexes: mTHPC/βCDp dilution 1:100 (blue); mTHPC/βCDp dilution 1:1000 (green); mTHPC/CMβCDp dilution 1:100 (red); mTHPC/CMβCDp dilution 1:1000 (purple); mTHPC/Me-β-CD dilution 1:100 (orange), mTHPC/Me-β-CD dilution 1:1000 (brown). The fluorescence of mTHPC was excited at 420 nm and registered at 652 nm.

Fig. 4. Mean fluorescence intensity (MFI) of mTHPC in 2D monolayer FaDu cells treated 24h with mTHPC (1 µg/mL) without CD polymers (■); in the presence of various concentrations of βCDp (●) and CMβCDp (●) in the culture medium. The concentration of FBS was 2 %. Data represent mean ± SD [n = 4; *p < 0.05, ***p < 0.001 using the t-test with Welch Correction]

Fig. 5. (**A**) Mean fluorescence intensities (MFI) and (**B**) Coefficients of Variation (CV) of mTHPC distribution between individual cells in 3D FaDu spheroids. Spheroids were treated 24h with mTHPC (3 µg/mL) without CD polymers (■) and in the presence of various concentrations of βCDp (●), and CMβCDp (●) in culture medium. The CV of mTHPC distribution in monolayer cells (♦) is presented for comparison. The concentration of FBS was 2 %. Data represent mean ± SD [n = 3; *p < 0.05, **p < 0.01 and ***p < 0.001 using the t-test with Welch Correction]

Fig. 6. The penetration of mTHPC in FaDu spheroid after 24h incubation in the presence of CD polymers. (**A**) Typical fluorescence images of spheroid cryosections after incubation with mTHPC (3 µg/mL) and various concentrations of βCDp and CMβCDp. The fluorescence is

displayed in red color (2D images and overlay brightfield/fluorescence photos) and in pseudo-colors (3D surface plots). (**B**) HES staining of spheroid cryosections. Scale bars indicate 100 µm.

Fig. 7. The penetration profiles of mTHPC in FaDu spheroids after 24h incubation in the presence of CD polymers. (**A**) Scheme of images processing and estimation of the mid-penetration depth (d_{50}). (**B&C**) Linear fluorescence profiles of mTHPC in FaDu spheroids after 24h incubation in the presence of (**B**) βCDp and (**C**) CMβCDp. (**D**) The penetration depth of 50% mTHPC (d_{50}) (box in FaDu spheroids treated with mTHPC alone (■) and in the presence of various concentrations of βCDp (●) and CMβCDp (♦). (**E**) Scatterplot of d_{50} versus MFI: mTHPC alone (■); mTHPC + βCDp (●) and mTHPC-CMβCDp (♦). The linear fit curve represents the correlation trend (solid line) with 95% confidential intervals (dashed lines). Data represent mean ± SD [n = 6 in (b − d), $^{**}p < 0.01$ compared to unembedded mTHPC, using ANOVA].

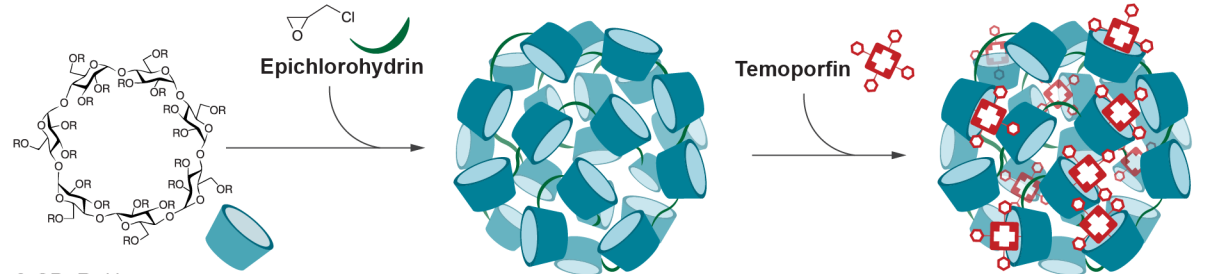
Epichlorohydrin
Cl
Temoporfin
β-CD: R=H
CM-β-CD: R=H21-m or (CH2COOH)m
CD polymer (nanosponge)

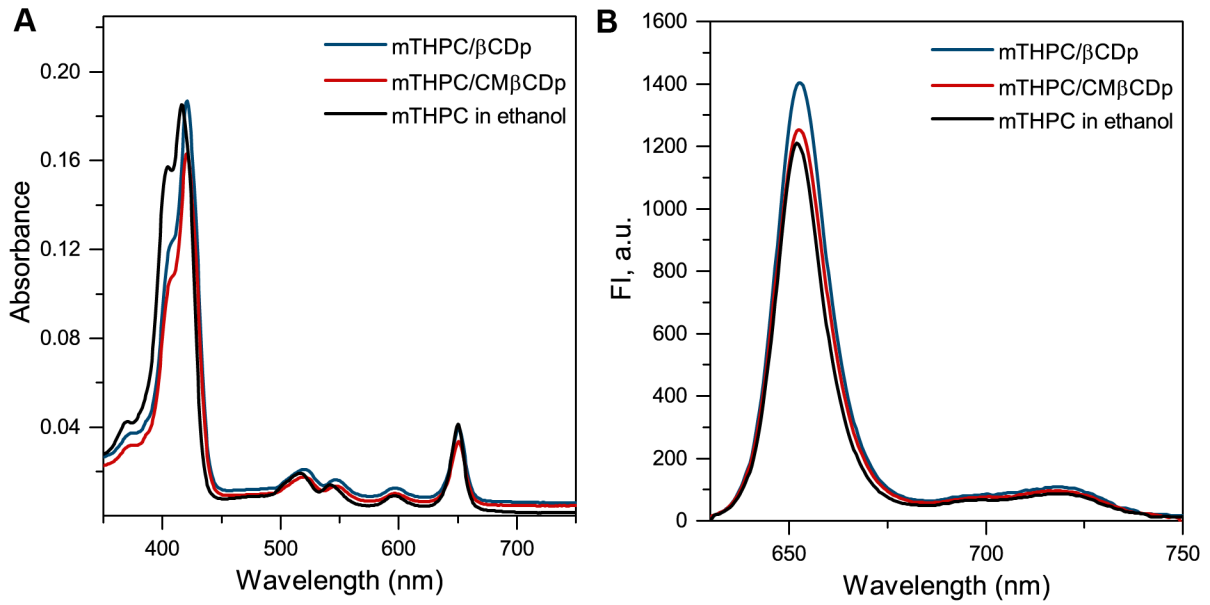
A
Absorbance
0.20
0.16
0.12
0.08
0.04
400
500
600
700
Wavelength (nm)
mTHPC/βCDp
mTHPC/CMβCDp
mTHPC in ethanol
B
FI, a.u.
1600
1400
1200
1000
800
600
400
200
0
650
700
750
Wavelength (nm)
mTHPC/βCDp
mTHPC/CMβCDp
mTHPC in ethanol

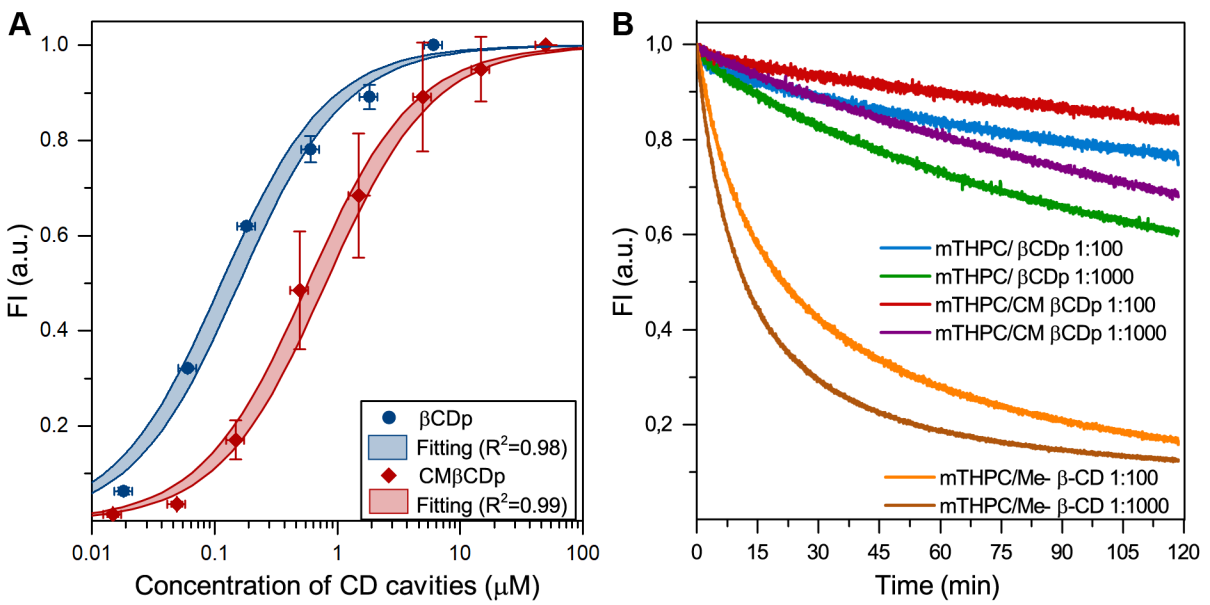
A
1.0
0.8
0.6
0.4
0.2
FI (a.u.)
0.01
0.1
1
10
100
Concentration of CD cavities (μM)
βCDp
Fitting (R²=0.98)
CMβCDp
Fitting (R²=0.99)
B
1,0
0,8
0,6
0,4
0,2
FI (a.u.)
mTHPC/ βCDp 1:100
mTHPC/ βCDp 1:1000
mTHPC/CM βCDp 1:100
mTHPC/CM βCDp 1:1000
mTHPC/Me- β-CD 1:100
mTHPC/Me- β-CD 1:1000
0
15
30
45
60
75
90
105
120
Time (min)

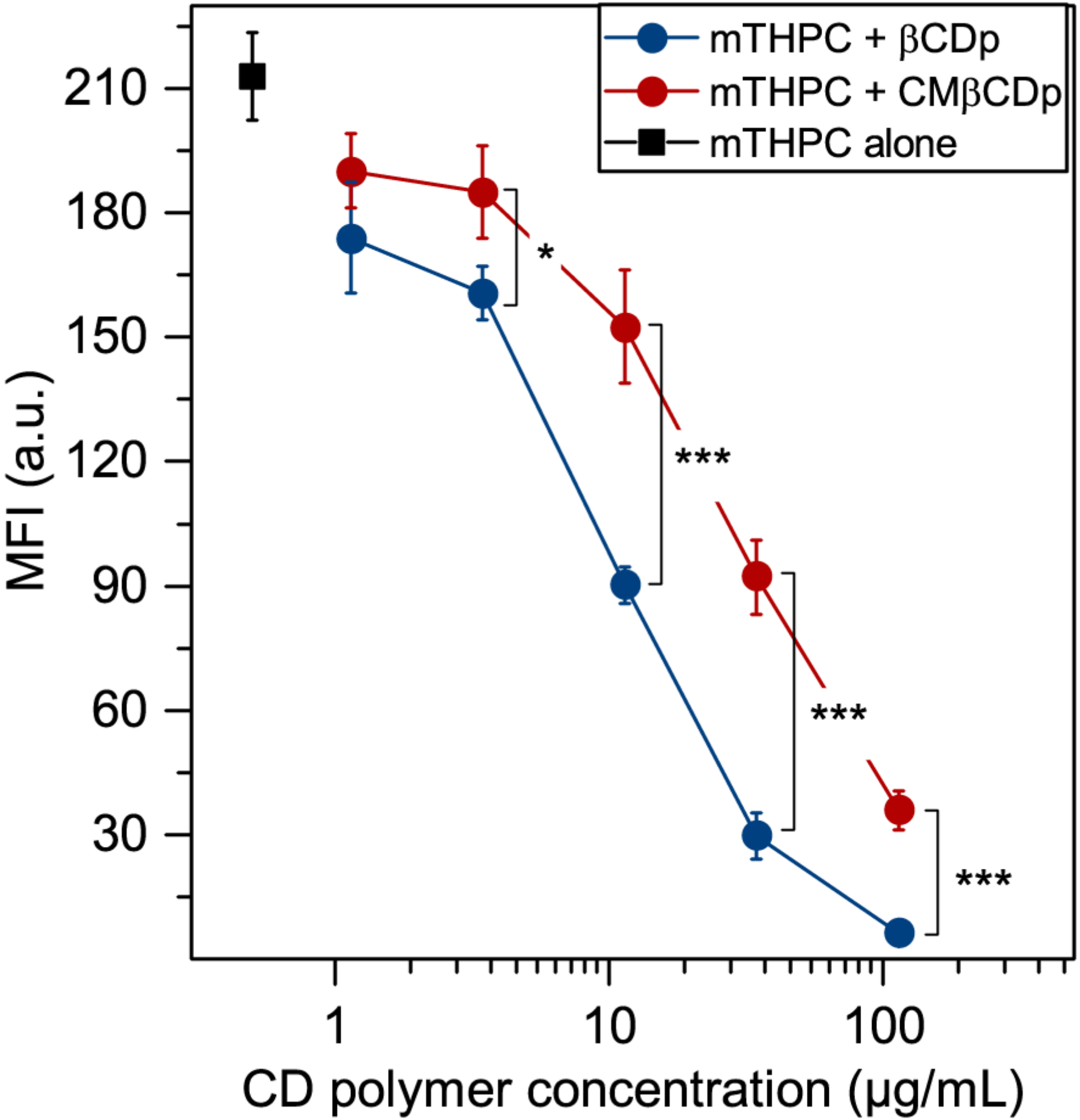
mTHPC + βCDp
mTHPC + CMβCDp
mTHPC alone
MFI (a.u.)
210
180
150
120
90
60
30
*
***
***
***
1
10
100
CD polymer concentration (µg/mL)

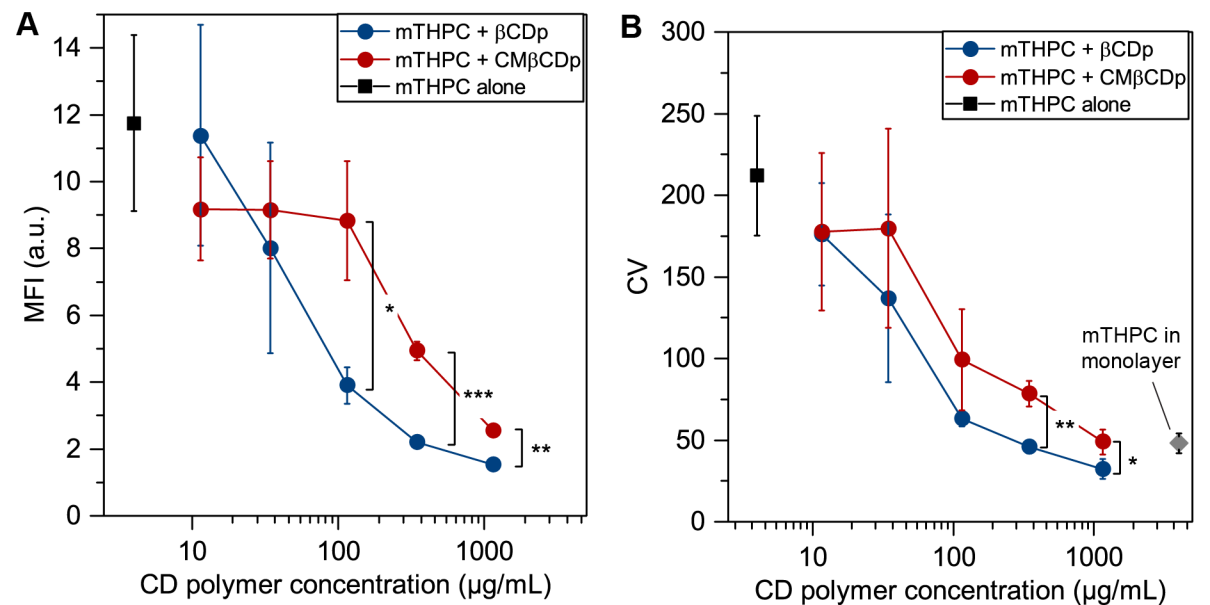
A
MFI (a.u.)
CD polymer concentration (µg/mL)
mTHPC + βCDp
mTHPC + CMβCDp
mTHPC alone
*
***
**
B
CV
CD polymer concentration (µg/mL)
mTHPC + βCDp
mTHPC + CMβCDp
mTHPC alone
mTHPC in monolayer
**
*

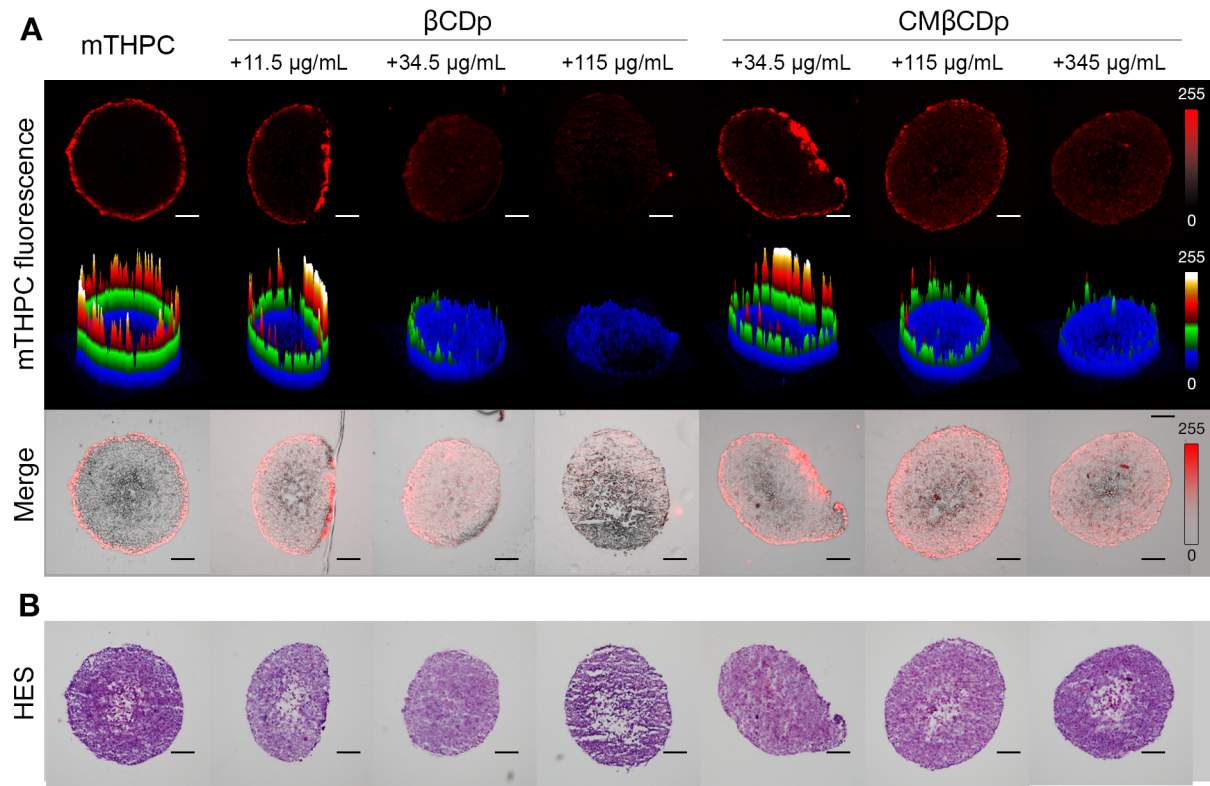
A
mTHPC
βCDp
+11.5 µg/mL
+34.5 µg/mL
+115 µg/mL
CMβCDp
+34.5 µg/mL
+115 µg/mL
+345 µg/mL
mTHPC fluorescence
Merge
255
0
B
HES

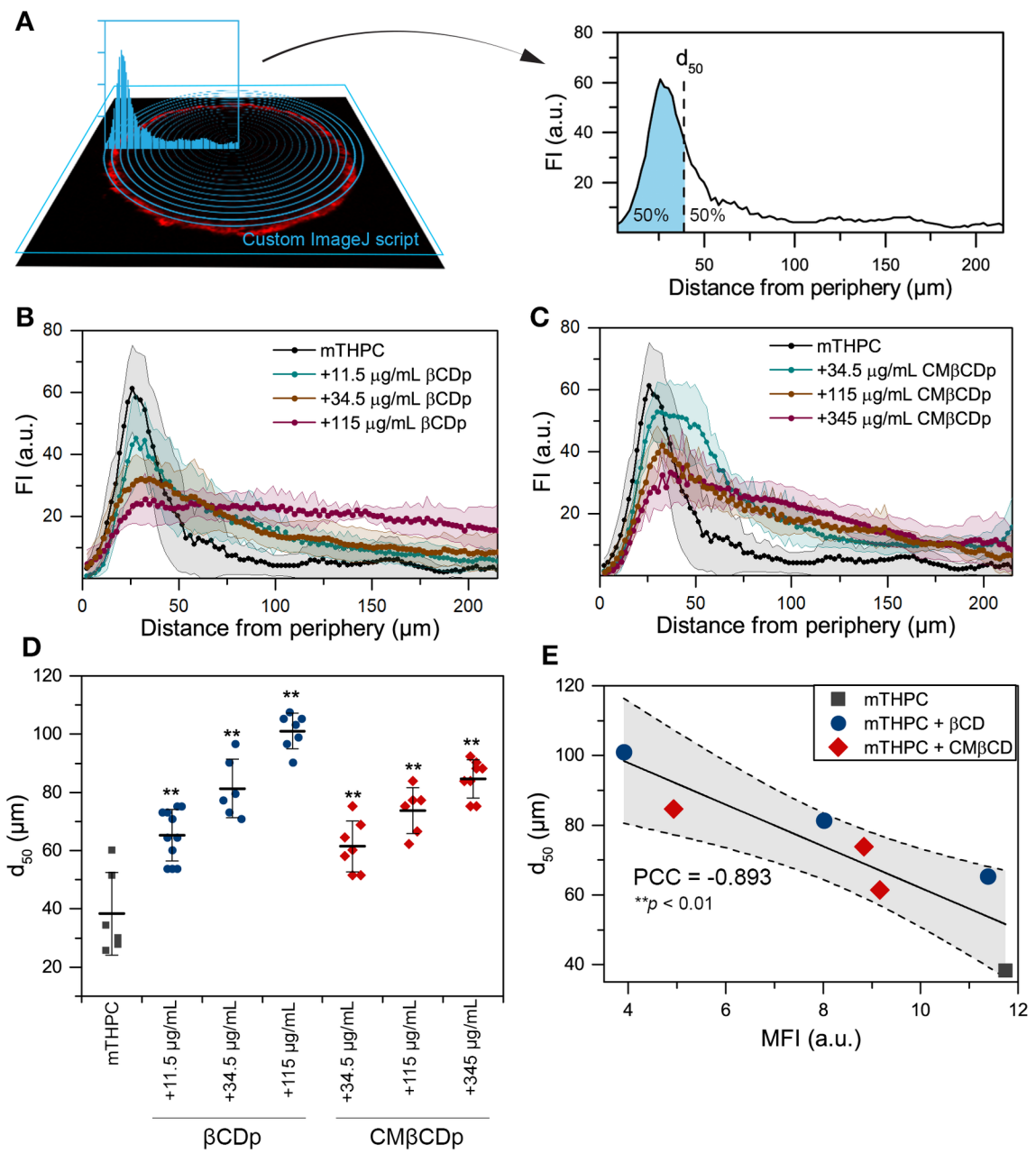
A
Custom ImageJ script
d50
FI (a.u.)
50%
50%
Distance from periphery (μm)
B
mTHPC
+11.5 μg/mL βCDp
+34.5 μg/mL βCDp
+115 μg/mL βCDp
FI (a.u.)
Distance from periphery (μm)
C
mTHPC
+34.5 μg/mL CMβCDp
+115 μg/mL CMβCDp
+345 μg/mL CMβCDp
FI (a.u.)
Distance from periphery (μm)
D
d50 (μm)
**
mTHPC
+11.5 μg/mL
+34.5 μg/mL
+115 μg/mL
+34.5 μg/mL
+115 μg/mL
+345 μg/mL
βCDp
CMβCDp
E
mTHPC
mTHPC + βCD
mTHPC + CMβCD
d50 (μm)
PCC = -0.893
**p < 0.01
MFI (a.u.)

Table 1. Spectral characteristics of mTHPC in CD polymers

	$\lambda_{Soret}/\lambda_{Q4}$ (nm)	ε_{650} ($cm^{-1}M^{-1}$)	$\lambda_{exc}/\lambda_{em}$ (nm)	FQY	*r*
mTHPC/βCDp	421/651	25 440	420/653	0.107 ± 0.004	0.147 ± 0.030
mTHPC/CMβCDp	421/651	24 280	420/653	0.089 ± 0.005	0.123 ± 0.010
mTHPC in ethanol	416/650	29 600*	416/652	0.092†	0.02†

* the data are taken from [14]
† the data are taken from [19]

Table 2. Characteristics of CD polymers

CD polymer	Size (nm)	PDI	CD units per NP
βCDp	45.3 ± 8.1	0.296±0.106	67-94
CMβCDp	59.3 ± 9.3	0.454 ± 0.080	56-78

Table 3. Decimal logarithmic values of apparent binding constants (*K*, unit: M^{-1}) of mTHPC with CD polymers, assuming 50% and 70% CD content in polymers

CD polymer	Log*K*	R^2
βCDp	6.79-6.94	0.98
CMβCDp	6.09-6.23	0.99

CD nanosponges increase Temoporfin penetration in spheroids at the cost of cellular uptake

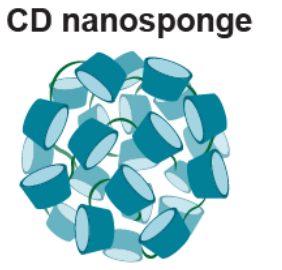

Concentration
of CD nanosponges

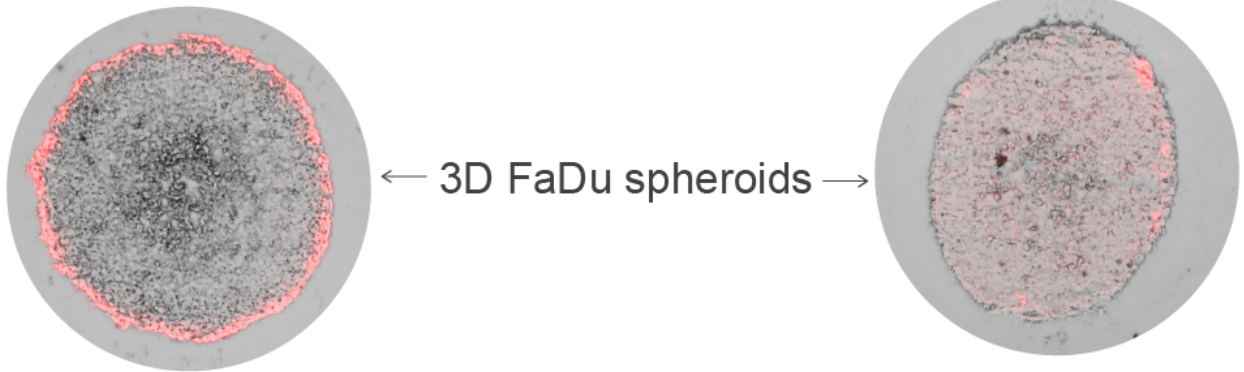

Temoporfin penetration

Temoporfin uptake